R. R. Chladny, C. R. Koch, and A. F. Lynch. Modeling of automotive gas-exchange solenoid valve actuators. *IEEE Transactions on Magnetics*, Volume 41, Issue 3:1155–1162, 2005. doi: 10.1109/TMAG.2004.841701

Modeling of Automotive Gas Exchange Solenoid Valve Actuators

Ryan R. Chladny, *Student Member, IEEE,* Charles Robert Koch, *Member, IEEE,*
and Alan F. Lynch, *Member, IEEE*

***Abstract*— A promising method for enhancing automotive engine efficiency uses solenoids to directly control the gas exchange valves of an internal combustion engine. A FEA (Finite Element Analysis) model is developed to describe transient and static operation of the valve. The FEA model is validated by experimental testing on an actual automotive prototype valve. We show that a nonlinear lumped parameter model which uses FEA results also closely matches experimental data. The lumped parameter model is amenable to optimization of design and can be readily used for closed-loop simulation. A simplified lumped parameter model is presented to facilitate controller design. Finally, a dynamic open-loop simulation is compared with experimental results.**

***Index Terms*— engines, solenoids, finite element method, modeling, magnetic losses, eddy currents.**

I. Introduction

It has been known as early as 1899 that having independent control over the timing of gas exchange valves of an internal combustion engine (ICE) can improve efficiency and performance [1]. Standard ICEs with fixed camshaft timing must compromise between low and high engine speed efficiency. Currently, a number of variable valve timing (VVT) actuators have been implemented on laboratory engines. These technologies include electrical motor [2], pneumatic [3], [4], hydraulic [5], [6], and solenoid actuators [7], [8]. Many of these approaches cannot provide sufficiently fast and precise control of cylinder charge during engine transients. An example of where the importance of transient cylinder charge control is critical occurs in combustion modes such as homogeneous charge compression ignition in spark ICEs. An example of a solenoid actuator is described in [9] and shown in Figure 1. Solenoids offer flexible valve timing resulting in precise regulation of transient cylinder charge. Power consumption, efficiency and consumer cost often provide the primary motivation for the development of new technologies. The electromagnetic valvetrain (EMV) is no exception. Although a production EMV, including the associated power electronics and generator, is estimated to increase the parasitic engine load by 1% over a conventionally driven cam-roller valvetrain [10], there is an immediate improvement of 15-20% in fuel economy through volumetric efficiency enhancement alone [11], [7], [12]. We expect the actuator used in this paper will have similar performance and energy consumption characteristics. The efficiency enhancement afforded by an EMV should be dramatic enough to motivate further research in enabling and cost sensitive fields such as power-electronics, sensors/controls and microprocessors [13], [14], [15], [16]. In addition, higher efficiency of the actuator itself can be attained through improved control strategies [17]. Efficient control of solenoids must also address a number of challenging problems common to most VVT approaches. Active control is required to prevent excessive valve seating velocity, premature wear and acoustic emissions [18], [19]. Solenoid valve control is also a challenge due to nonlinear effects such as magnetic saturation and system uncertainties including large disturbance forces from combustion pressure and parameter variation due to temperature change and component wear.

A number of designs for solenoids have been proposed. Typically the solenoid actuator consists of a linear-moving armature with two coils and two preloaded springs as shown in

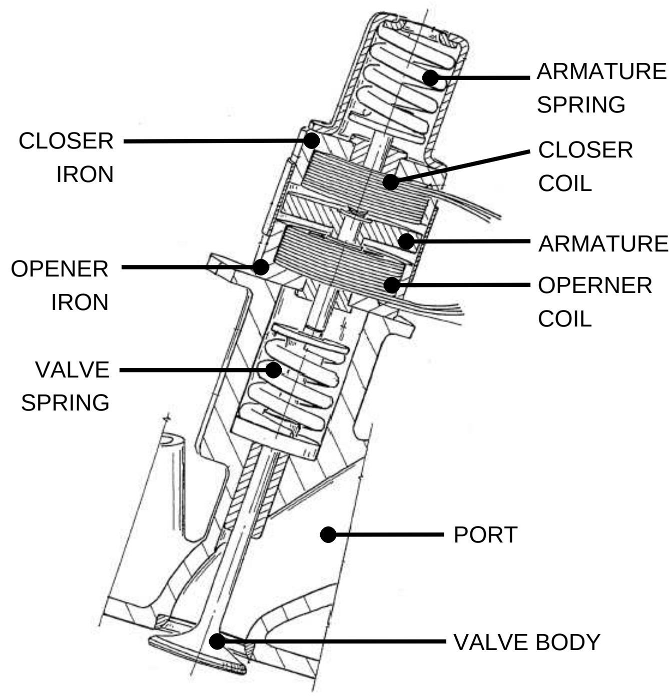

Fig. 1. Schematic of prototype solenoid valve actuator [9]

Manuscript received September 26, 2003; revised September 27, 2004.

This work was supported in part by the Natural Sciences and Engineering Research Council of Canada, under Research Grant numbers 249553-02, 249681-02.

The authors would like to thank DaimlerChrysler for the donation of the solenoid valves.

R.R. Chladny and C.R. Koch are with the Department of Mechanical Engineering, University of Alberta (e-mail: rchladny@ualberta.ca; bob.koch@ualberta.ca).

A.F. Lynch is with the Department of Electrical and Computer Engineering, University of Alberta (e-mail: alanl@ee.ualberta.ca).

Figure 1. The springs can achieve rapid flight times while minimizing electrical energy input and are essential in overcoming the significant combustion pressures. The electromagnets are required for "catching" the armature at either stroke bound. In addition, they are used to overcome friction and pressure disturbances. Permanent magnets have also been employed to "catch" the armature at the stroke bounds with electromagnets providing a release force [20], [21]. Other designs include hinged or clapper-type configurations [22].

Existing work on solenoid valve modeling includes methods based on reluctance networks [23] and FEA [24], [25], [26]. In the reluctance network method, the device flux path is approximated and characterized through material properties and geometry. The result is a magnetic circuit in which each of the distinct device regions constitute an element. Solving the circuit allows for the calculation of flux density in any particular region from which a mechanical force can be derived. It is often difficult for such models to include flux fringing, leakage, and material saturation. FEA-based modeling approaches usually do not simultaneously predict electric, magnetic, and mechanical responses. Even using software where this is possible [27], the computational time required for obtaining the system response is impractical. For this reason, this paper demonstrates the advantage of incorporating FEA in a LP (lumped parameter) model which accurately predicts the system response and can be readily used for control design or solenoid optimization.
This paper is organized as follows: Section II describes the prototype actuator and its FEA model for simulating steady state (fixed position and constant current) and transient voltages at a fixed armature position. In Section III, FEA results are incorporated into a LP model. Next, a simplified LP model which is convenient for control design is derived. Section IV compares the transient responses for the LP and FEA models. Section V contrasts a dynamic simulation with experimental data. Finally, conclusions are drawn in Section VI.

II. FEA Modeling

A. Actuator Description

A prototype actuator similar to the one described in [9] and shown in Figure 1, has been donated by Daimler-Chrysler. This linear actuator is characterized by a short stroke, small air gap, and flat pole and armature geometries. The flat-face, short-stroke properties allow for faster response at larger air gaps in addition to stronger holding forces due to increased flux density. Although a variety of pole and armature geometries are conceivable (such as conical or I-shaped), the flat-face offers a large surface area and minimal fringing for maximum force density [28]. Other configurations such as conical pole/armature interfaces produce greater fringing, resulting in a more linear force-position relationship but sacrifice force density. Another key design characteristic of the prototype actuator is the use of two preloaded linear compression springs. These springs are used to achieve rapid flight times while minimizing electrical power input by storing kinetic energy during valve deceleration. Thus, the electromagnets are only required for "catching" the armature at either end of

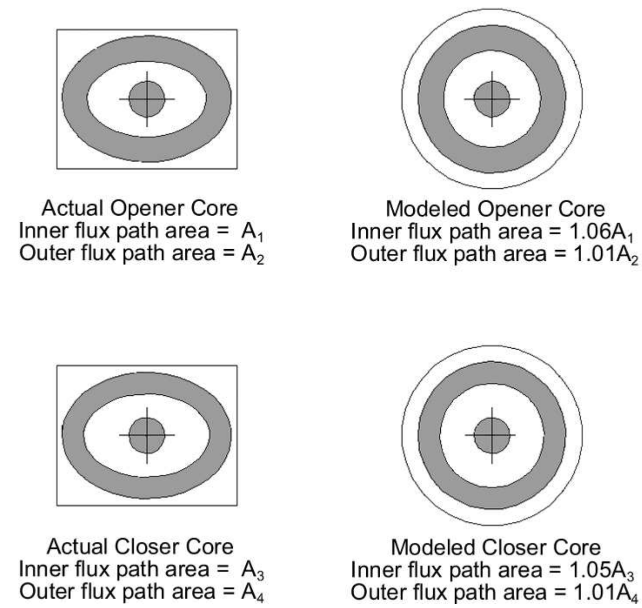

Fig. 2. Contrast of actual vs. modeled actuator flux path section areas

the stroke as well as overcoming friction and pressure forces. The mechanical system of the actuator can be considered as a mass-spring oscillator with an undamped natural frequency of approximately $150-200$ Hz. This resonant frequency largely determines the duration of valve flight (damped period of about 8ms) and is a function of the desired maximum engine speed. In a traditional cam-driven valvetrain, the valve flight time and timing are directly proportional to engine speed. In the case of a solenoid actuator, these properties are independent of engine speed and position. The natural frequency of the actuator considered here is selected for a maximum engine speed of about 5500 RPM. A constant lift trajectory independent of engine speed adversely affects engine performance at low RPM. Efforts have been made to address this issue through partial opening of the valve or "mini-lift" at lower engine speeds [29] and cylinder deactivation [7], [30]. The core and armature of the actuator used in this study are comprised of silicon-steel sintered-powder metallurgical castings. The fine grain structure of this material inhibits eddy currents. The core is liquid cooled to minimize ohmic losses and thermal parameter variation. The silicon steel has a conductivity of approximately 1.4 MS/m and a relative permeability of 1000.

B. Modeling Assumptions

Two dimensional representations of the opener and closer are separately modeled assuming vertical symmetry to minimize model complexity and computational time. This assumption implies that the actuator has a cylindrical as opposed to its actual elliptical cross-section. Figure 2 illustrates the actual and modeled cross-sections (normal to the air gap flux path) that will most influence force estimates. Using 2D axisymmetric geometry for the 3D actuator assumes that fringing in the corners of the back iron and armature, and the more complex 3D eddy current paths during transients, are negligible. The above simplifications will be shown to have

TABLE I
AIR GAP AND EXCITATION OPERATING POINTS

Air Gap [mm]

0.04	0.08	0.15	0.20	0.30	0.40	0.50	0.60
0.80	1.00	1.50	2.00	3.00	4.00	6.00	8.00

Coil Excitations / MMF [Ampere-turns]

50	100	150	200	250	300	400
500	600	800	1000	1500	2000	2500
3000	3500	4000	4500	5000	5500	6000

modest effect on model accuracy; less than 13% error. Our model considers only the opener component without modeling the closer. We ignore the closer due to the high permeability of the armature and since in practice only one coil is active at any time.

C. FEA method

We apply an FEA method which uses a magnetic vector potential [27]. This method is used for static and transient analyzes with a quasi-static limit. The following Maxwell equations are used:

$$\nabla \cdot \boldsymbol{E}(\mathbf{r},t) = \frac{\rho(\mathbf{r},t)}{\epsilon_0} \quad (1)$$

$$\nabla \times \boldsymbol{B}(\mathbf{r},t) = \mu \boldsymbol{J}(\mathbf{r},t) \quad (2)$$

$$\nabla \times \boldsymbol{E}(\mathbf{r},t) = -\frac{\partial \boldsymbol{B}(\mathbf{r},t)}{\partial t} \quad (3)$$

$$\nabla \cdot \boldsymbol{B}(\mathbf{r},t) = 0 \quad (4)$$

Where $\boldsymbol{E}$ is electric field, $\boldsymbol{B}$ is magnetic flux density, $\boldsymbol{J}$ is current density, $\mu(H)$ is the scalar field dependent magnetic permeability (isotropic material assumed), ρ is volumetric charge density, and ϵ_o is electric permittivity of free space.

Denoting magnetic field intensity by $\boldsymbol{H}$ and electrical conductivity by σ we have

$$\mu(\boldsymbol{H})\boldsymbol{H} = \boldsymbol{B}, \quad \boldsymbol{J} = \sigma \boldsymbol{E} \quad (5)$$

to describe material behavior assuming no temperature dependence or relative motion.

Using (1)–(5) and a Coulomb gauge condition, the FEA software solves the following three equations:

$$-\nabla^2 \boldsymbol{A} = \mu(\boldsymbol{H})\boldsymbol{J}(\boldsymbol{r},t)$$

$$\nabla \cdot \left(\frac{\partial \boldsymbol{A}}{\partial t} - \nabla P\right) = 0$$

$$\sigma \frac{\partial \boldsymbol{A}}{\partial t} - \frac{1}{\mu(\boldsymbol{H})}\nabla^2 \boldsymbol{A} + \sigma \nabla P = 0$$

Where $\boldsymbol{A}$ denotes vector magnetic potential and P denotes the electrical potential. In the case of axisymmetry, the vector potential $\boldsymbol{A}$ has only one nonzero component.

1) Static Modeling and Simulation: Static models of the opener and closer are created. For each operating point, appropriate geometry, mesh, material properties, boundary conditions and current excitations are set and the resulting force and flux data saved. Results for the opener are determined for

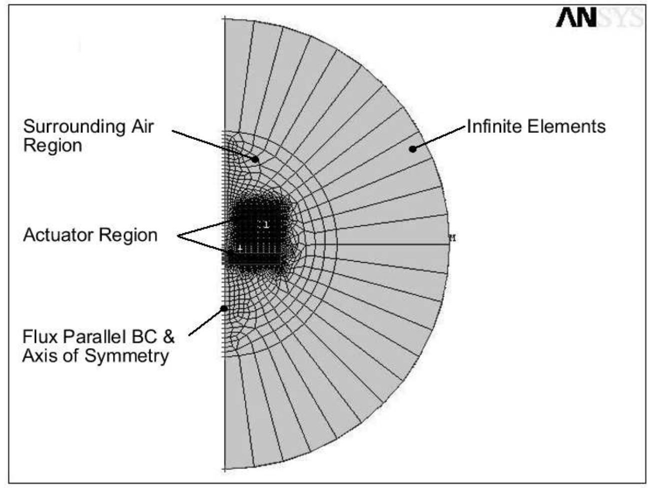

Fig. 3. Static model elements and mesh

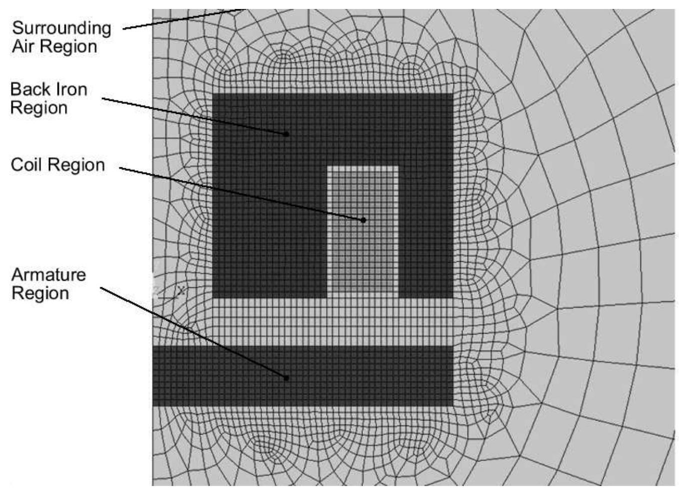

Fig. 4. Close-up of static and transient model elements and mesh

each of the operating points listed in Table I for a total of 336 static solutions. The operating points were selected to provide a relatively smooth force and flux relation as a function of air gap and current. A higher number of data points are required for a smooth data set at low air gaps due to the dramatic change in magnetic flux and force in these regions. Similarly, due to material saturation, a higher resolution of data is required at lower excitation. Mesh refinement is determined by inspection as well as by ensuring force and flux convergence with respect to an increase in element density. In order to prevent elements with poor aspect ratios, active mesh control was established in the back iron, armature and air gap regions in addition to the model boundaries. The default auto-mesh generator was used to mesh the remaining regions with the finest mesh refinement possible. In order to ensure appropriate element densities and shapes at extreme armature positions, a linear function was used to control the element mesh in the air gap region over the 8 mm range of motion.

For both iron and air regions, 2D quadrilateral elements with a magnetic potential degree of freedom are used. Figures 3

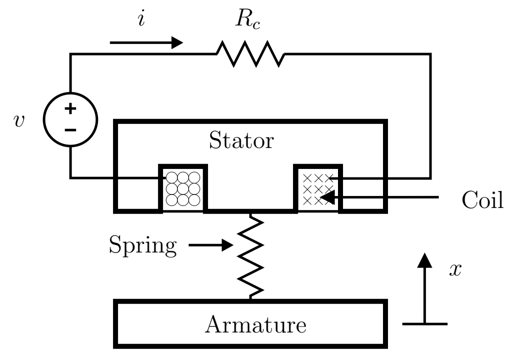

Fig. 5. Schematic of the solenoid actuator valve

and 4 illustrate a typical element mesh over the armature, air and back iron. A single layer of boundary elements is used around the perimeter of the model (excluding the axis of symmetry) to model far field decay. These infinite elements use shape functions which require the magnetic potential to be zero at infinity. Coil excitation is applied directly to the coil elements in the form of current density. Nodes located on the line of symmetry are constrained to zero magnetic potential (flux parallel or Dirichlet boundary condition). Validity of the model is assessed by comparing simulation results to experimental measurements (see Section IV-A).

2) Transient Modeling and Simulation: The transient behavior of the model is determined by applying a voltage step at a constant air gap to a quasi-static transient FEA model. A step voltage is chosen as it is a typical output waveform of driver circuits [31], [32], [8]. Quadrilateral elements with additional EMF and current degrees of freedom are used for circuital excitation and to account for transient effects such as eddy currents. A voltage source, resistor, and stranded coil element are modeled to excite the actuator finite element domain. The circuit elements are not part of the field solution. Rather, the stranded coil element's current and EMF degrees of freedom are coupled to the coil elements in the actuator domain. The coil resistance, assumed independent of temperature, is accounted for through the geometry of the FEA and the specified conductivity of copper. An approximate step waveform voltage, measured from an actual experiment, was applied to the FEA model for ease of comparison with experimental data (see Section IV).

III. Nonlinear Lumped Parameter Model

The LP model is an ordinary differential equation which facilitates prediction of system performance without the computational burden of FEA. The LP model will be shown to provide reliable system trajectories once it is parameterized using static and transient FEA results. The armature position of the solenoid valve system, shown schematically in Figure 5, is denoted by x and the origin of the x-coordinates is defined at the midpoint between the two coils. The armature is mechanically constrained to move on $x \in [-4, 4]$ mm. As mentioned before, only one coil in isolation is considered.

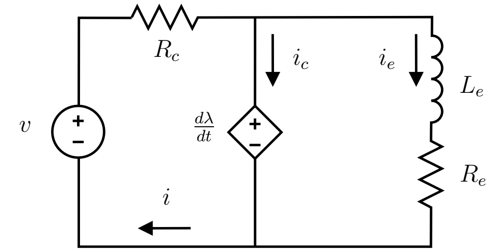

Fig. 6. Modeled circuit diagram

A. LP Model

A schematic of the system is shown in Figure 5, and the circuit used to model the electrical subsystem is shown in Figure 6. Circuit analysis and Newton's law gives:

$$\frac{d\lambda}{dt} = v - R_c\left(i_e + i_c(\lambda, x)\right) \tag{6}$$

$$\frac{di_e}{dt} = \frac{1}{L_e}\left(v - R_c(i_e + i_c(\lambda, x)\right) - R_e i_e \tag{7}$$

$$m\ddot{x} = F_m(i_c(\lambda, x), x) + \mathcal{A}(x, \dot{x}) \tag{8}$$

Where v is the input voltage applied to the coil, R_c is the resistance of the coil, i_c is the coil current, and λ is the flux linkage. To model eddy current effects, a parallel branch including a resistor R_e and inductor L_e is included with current flowing in this branch denoted by i_e. We remark that velocity induced eddy currents are not included in the model for several reasons. The estimated skin depths caused by transient coil currents are approximately 1 mm while those predicted by armature velocity exceed the core dimensions. Physically, this is to be expected as velocities are relatively low (< 0.5 m/s) in the regions close to the pole faces, where motion control is executed. The assumption that transient excitation losses are dominant in contrast to those induced by armature motion is validated with empirical observation is Section V. Friction and spring force effects are included in $\mathcal{A}(x, \dot{x}) = -(k_s x + B\dot{x})$, where $k_s x$ is the restoring force due to both springs with an effective stiffness k_s, $B\dot{x}$ is viscous frictional force of the mechanism, and m is the effective moving mass. The magnetic force exerted on the armature is denoted by $F_m(i_c, x)$. Steady state FEA results provide magnetic force and flux linkage data as a function of x and i_c and the evaluation of (6)–(8) is accomplished using lookup tables. The parameters R_e and L_e are determined from transient FEA step voltage simulations.

B. Simplified LP Model

The LP model (6)–(8) is further simplified by assuming no magnetic saturation, leakage flux or eddy currents. These assumptions result in the electromagnet having an inductance of the form:

$$L(x) = 2\beta/(\kappa - x)$$

Where β and κ are related to the number of turns, area and lengths of the flux paths, and magnetic permeabilities of the air and iron core of the coil. Again it is assumed that this

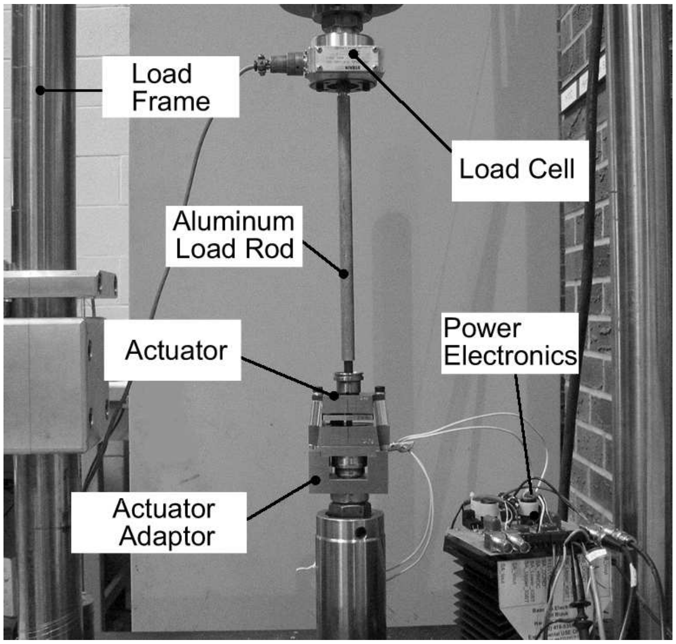

Fig. 7. Experimental setup

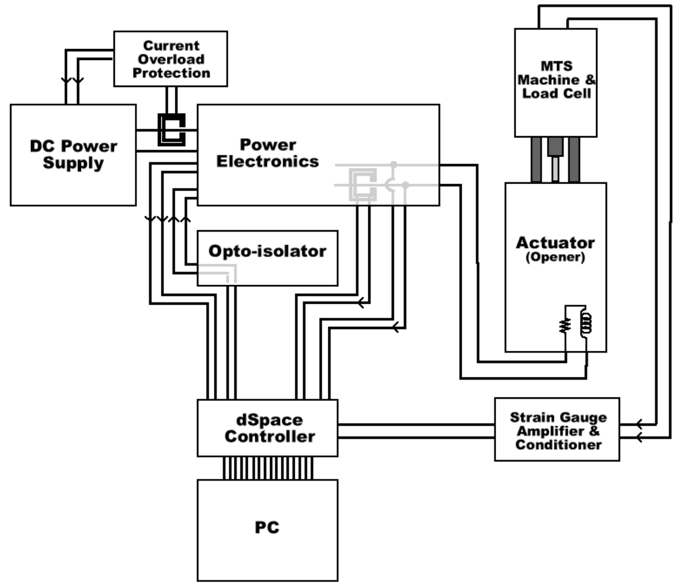

Fig. 8. Schematic of the experimental setup

model has no coupling between the coils. The force F_m is obtained by differentiating the coenergy function

$$W(x,i) = \int_0^i \lambda(x,\xi)d\xi$$

with respect to position, where $\lambda(x,i) = L(x)i$ is the flux linkage of the coil, and $i = i_c$ is the coil current. Thus, the force equation is:

$$F_m(x,i) = \frac{\partial W}{\partial x}(x,i) = \int_0^i \frac{\partial \lambda}{\partial x}(x,\xi)d\xi = \frac{\beta i^2}{(\kappa - x)^2} \quad (9)$$

Substituting this expression into Newton's law (8) gives:

$$\ddot{x} = \frac{\beta}{m}\frac{i^2}{(\kappa - x)^2} + \frac{\mathcal{A}(x,\dot{x})}{m} \quad (10)$$

The differential equation for i is:

$$\frac{di}{dt} = \frac{\kappa - x}{2\beta}(v - Ri) + \frac{\dot{x}i}{\kappa - x} \quad (11)$$

The parameters R, m, B, and k_s can be readily measured from the system. Parameters κ and β are obtained from a least squares fit to the force data obtained from the FEM model described in Section II. Relative to (6)–(8), the simplified model (10) and (11) is amenable to model-based control methods [33].

IV. Equipment & Experimental Setup

To validate the FEA and LP model (6)–(8), steady state and transient measurements are performed [34]. The experimental setup is shown in Figures 7 and 8. A 50 kHz pulse width modulation (PWM) current controller was used to regulate coil current.

A. Static Experiments

For the steady-state force, constant current was input to the coil. To avoid overheating the coil, excitation levels are limited to 40A. The static force results are plotted in Figure 9 as lines of constant mmf. This nonlinear force response is indicative of the flat pole face armature actuator type. Experimental results beyond $x = 4$ mm are not included due to load cell resolution at low loads. At higher values of mmf in Figure 9 the curves shown deviate from $\beta i^2/(\kappa - x)^2$ in (9). This deviation indicates onset of magnetic saturation [35].

B. Transient Experiments

In order to validate the accuracy of the FEA model results to voltage transients, several experiments are conducted that measure actuator force and current response to a voltage pulse input. A 1.5 ms voltage pulse is applied to the coil while the armature is held at a constant position using a material testing machine. This process is repeated with increasing pulse amplitudes of 24 V, 42 V, and 50 V over the full range of air gaps. As shown in Figure 10, experimental results are used as an input to the simulation. The experimental and simulated current and force are compared in Figures 11 and 12 for a 1.5 ms, 42 V pulse at a fixed air gap of 0.5 mm.

The small oscillatory response of the experimental force curve shown in Figure 12 suggests a resonant mode of the actuator or load cell structure due to the applied load pulse. Video images of the experiments reveal significant armature deflection, resulting in a nonuniform and smaller average air gap. Thus the measured peak forces are approximately 13% higher than the FEA predictions.

Similar results for other air gaps also show close agreement between simulation and experiment. At air gaps less than 0.2 mm, the impulse force resulted in the armature to contact the pole face. Correct force measurements could not be obtained for such positions.

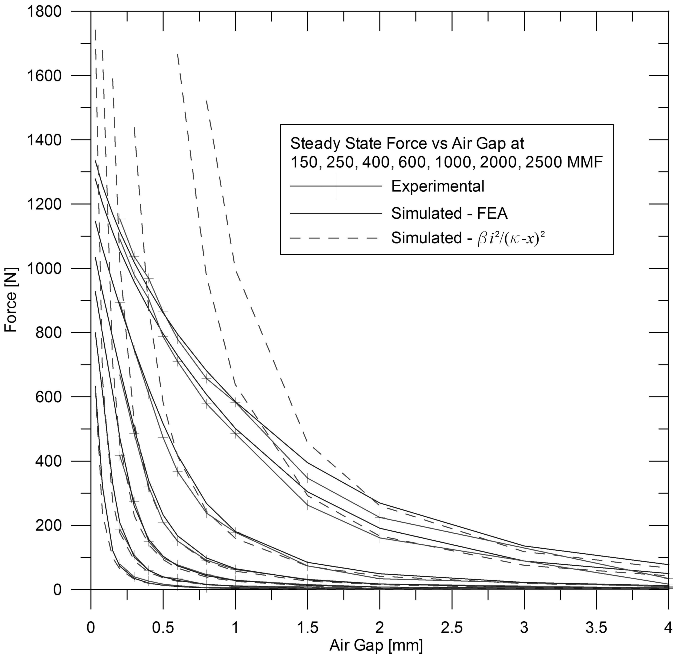

Fig. 9. Experimental and simulated force vs. air gap for various excitations

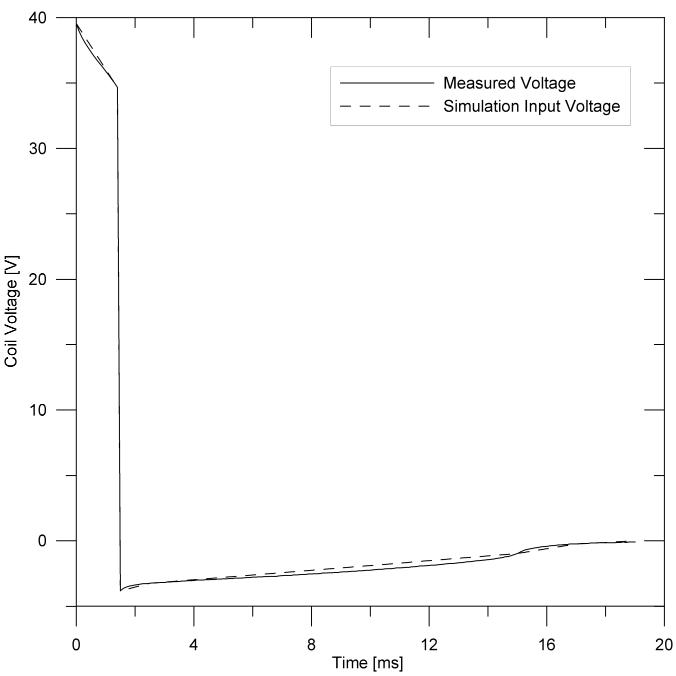

Fig. 10. Measured and input voltage, 1.5 ms, 42 V pulse at 0.5 mm air gap

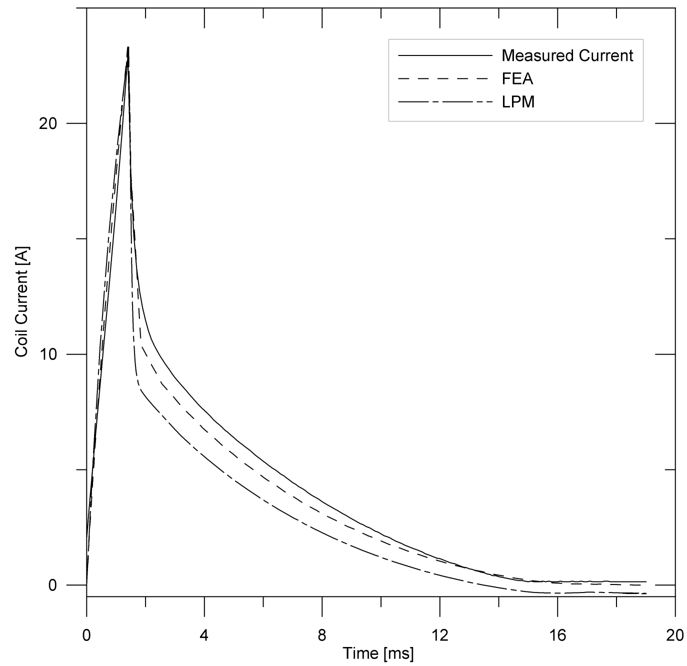

Fig. 11. Coil current response to a 42 V, 1.5 ms voltage pulse at 0.5 mm air gap

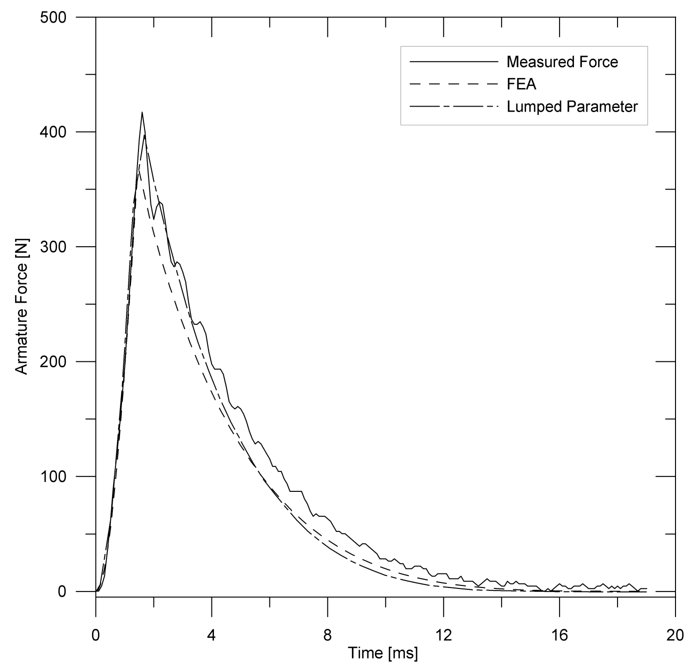

Fig. 12. Armature force response to a 42 V, 1.5 ms voltage pulse at 0.5 mm air gap

Three input voltage waveforms of different amplitude were investigated – see Figure 13. The resulting FEA and experimental currents and forces are compared in Figures 14 and 15. The results show close agreement between FEA and experimental data.

V. Dynamic Simulation

A complete dynamic simulation using the developed hybrid FEA/LP model is implemented and contrasted with an open loop experiment. In addition to eddy current and electromechanical modeling, the simulation also includes a simplified power electronics model. The power electronics are modeled using the Matlab/Simulink SimPower Systems toolbox and circuital physical parameters provided by the component manufacturers' specifications. The experimental test equipment and setup is described in [34]. Figure 16 illustrates the model performance of the opener magnet in contrast to

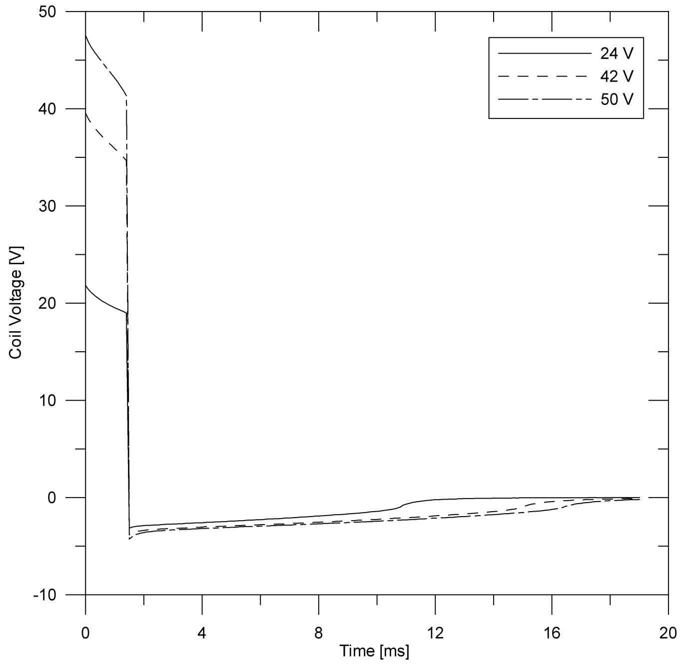

Fig. 13. Applied 1.5 ms, 24 V, 42 V and 50 V pulses at 0.5 mm air gap

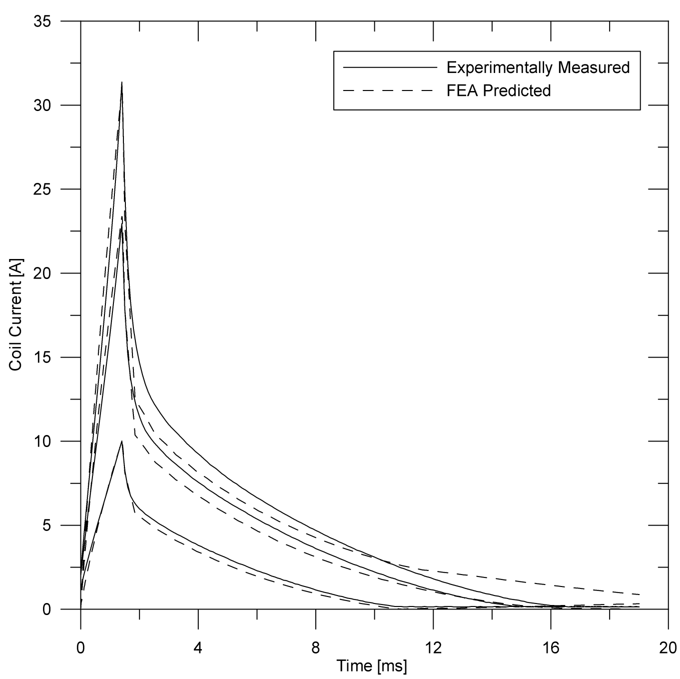

Fig. 14. Coil current response due to a 24 V, 42 V and 50 V, 1.5 ms pulse at 0.5 mm air gap

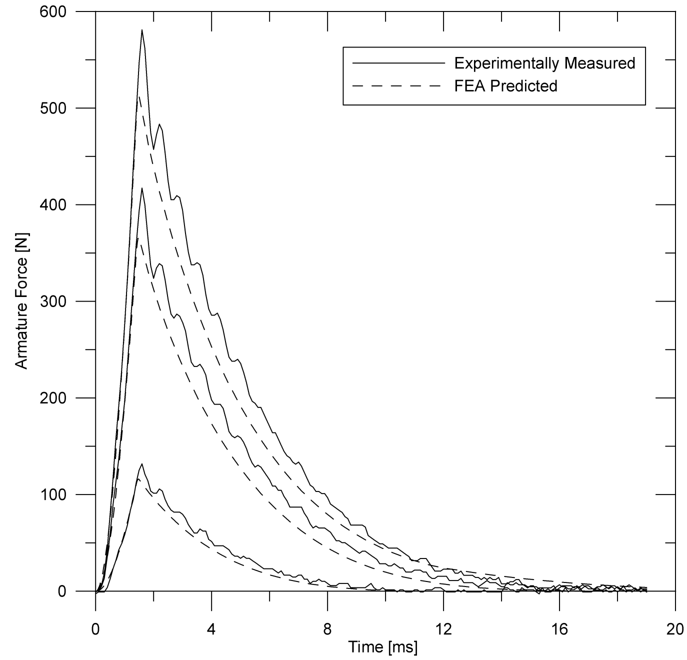

Fig. 15. Armature force response due to a 24 V, 42 V and 50 V, 1.5 ms pulse at 0.5 mm air gap

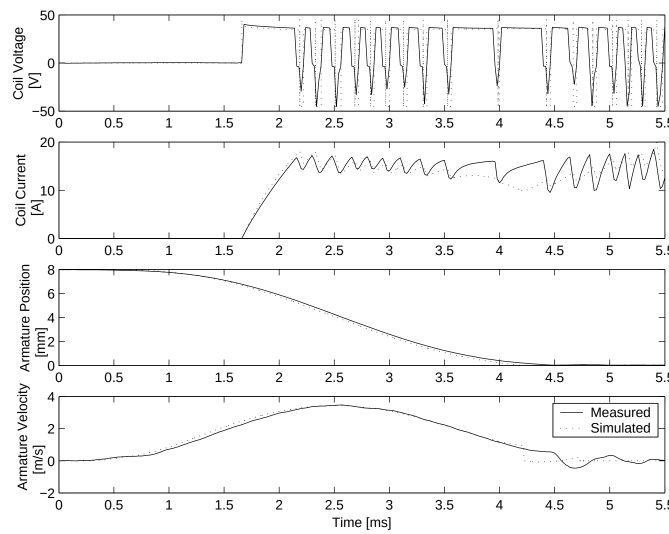

Fig. 16. Dynamic simulation and experimental results of the opener magnet

experimentally obtained results. In this case, no closed loop control is implemented and the armature is simply released from the closer magnet and caught with the opener using a constant current command. The simulation experimentally measured inputs are the digital signals used to switch the actual power electronics and the initial closer holding current value. In this instance, the supply voltage was switched between $\pm 42V$. The power supply simulated is ideal, which, along with circuital idealizations, account for the differences in voltage and current signals. Despite these idealizations, the simulation and experimental results are close, suggesting that this model can be used to evaluate control strategies accurately.

VI. Conclusion

The nonlinear uncertain dynamics and stringent performance requirements of solenoid valve actuators make modeling and control of these devices a challenging problem. In this paper a FEA model is used to generate experimentally accurate static force and flux data as well as voltage transient data for a real prototype actuator. The static force and flux data of the FEA model is used in a LP model which includes eddy current effects. The trajectories of the FEA and LP models are shown to be in good agreement with experimental results. A simplified model of the solenoid actuator is described. Finally, a dynamic simulation using the FEA derived LP model is contrasted with an open loop test case. Our results indicate that the FEA-based LP model (6)–(8) can be used as a plant model for simulating model-based control algorithms. Future work will concentrate on using the developed models for controller design and implementation on a single-cylinder research engine.

REFERENCES

[1] D. Payne, “Electically controlled valve gear for gas or other motors,” *U.S. Patent 623,821*, 1899.

[2] R. Henry, “Single-cylinder engine tests of a motor-driven variable-valve actuator,” *SAE paper 2001-01-0241*, 2001.

[3] W. Richeson and F. Erickson, “Pneumatic actuator with permanent magnet control valve latching,” *U.S. Patent No. 4,852,528*, 1989.

[4] L. Gould, W. Richeson, and F. Erickson, “Performance evaluation of a camless engine using valve actuators with programmable timing,” *SAE paper 910450*, 1991.

[5] J. Allen and D. Law, “Production electro-hydraulic variable valve-train for a new generation of I.C. engines,” *SAE paper 2002-01-1109*, 2002.

[6] S. Barros da Cunha, J. Hedrick, and A. Pisano, “Variable valve timing by means of a hydraulic actuation,” *SAE paper 2000-01-1220*, 2000.

[7] M. Pischinger, W. Salber, F. van der Staay, H. Baumgarten, and H. Kemper, “Benefits of the electromechanical valve train in vehicle operation,” *SAE paper 2000-01-1223*, 2000.

[8] B. Lequesne, “Fast acting, long-stroke solenoids with two springs,” *IEEE Trans. Ind. Applicat.*, vol. 26, pp. 848–856, 1990.

[9] P. Gladel, F. Kreitmann, O. Meister, T. Stolk, and A. V. Gaisberg, “Aktor zur elektromagnetischen Ventilsteuerung,” *German Patent Application DE19961608 A1*, 1999.

[10] R. Flierl and M. Klüting, “The third generation of valvetrains - New fully variable valvetrains for throttle-free load control,” *SAE paper 2000-01-1227*, 2000.

[11] D. Moro, F. Ponti, and G. Serra, “Thermodynamic analysis of variable valve timing infuence on SI engine efficiency,” *SAE paper 2001-01-0667*, 2001.

[12] T. Lancefield, R. Gayler, and A. Chattopadhay, “The practical application and effects of a variable event valve timing system,” *SAE paper 930825*, 1993.

[13] M. Fairchild, J. Myers, J. Badgett, C. Berlin, and D. Sarma, “Comparing substrate solutions for automotive power electronics applications,” *SAE paper 2004-01-1681*, 2004.

[14] M. Montanari, F. Ronchi, C. Rossi, and A. Tonielli, “Control of a camless engine electromechanical actuator: Position reconstruction and dynamic performance analysis,” *IEEE Trans. Ind. Electron.*, vol. 51, pp. 299–311, 2004.

[15] W. Hoffmann and K. Peterson and A. Stefanopoulou, “Iterative learning control for soft landing of electromechanical valve actuator in camless engines,” *IEEE Trans. Contr. Syst. Technol.*, vol. 11, pp. 174–184, 2003.

[16] S. Ernest, “When to integrate or not to integrate - A VVA system decision,” *SAE paper 2003-01-0031*, 2003.

[17] C. Gunselmann and J. Melbert, “Improved robustness and energy consumption for sensorless electromagnetic valve train,” *SAE paper 2003-01-0030*, 2003.

[18] Y. Wang, “Camless engine valvetrain: Enabling technology and control techniques,” *Ph.D. thesis, University of California at Santa Barbara*, 2001.

[19] J. Savage and J. Matterazzo, “Application of design of experiments to determine the leading contributors to engine valvetrain noise,” *SAE paper 930884*, 1993.

[20] B. Lequesne, “Design and optimization of two-spring linear actuators,” *European Trans. on Electrical Power*, vol. 9, pp. 377–383, 1999.

[21] M. Theobald, B. Lequesne, and R. Henry, “Control of engine load via electromagnetic valve actuators,” *SAE paper 940816*, 1994.

[22] Y. Kawase, H. Kikuchi, and S. Ito, “3-D nonlinear transient analysis of dynamic behavior of the clapper type DC magnet,” *IEEE Trans. Magn.*, vol. 27, no. 5, pp. 4238–4241, 1991.

[23] C. Chillet and J. Voyant, “Design-oriented analytical study of a linear electromagnetic acutator by means of a reluctance network,” *IEEE Trans. Magn.*, vol. 37, pp. 3004–3011, 2001.

[24] J. Brauer and J. Ruehl, “Coupled nonlinear electromagnetic and structural finite element analysis of an actuator excited by an electric circuit,” *IEEE Trans. Magn.*, vol. 31, pp. 1861–1864, 1995.

[25] K. Sraini and M. Féliachi, “Electromagnetic actuator behavior analysis using finite element and parametrization methods,” *IEEE Trans. Magn.*, vol. 31, pp. 3497–3499, 1995.

[26] S. Wang, T. Miyano, and M. Hubbard, “Electromagnetic field analysis and dynamic simulation of a two-valve solenoid actuator,” *IEEE Trans. Magn.*, vol. 29, pp. 1741–1746, 1993.

[27] *ANSYS theory reference*, ANSYS Inc., 2002, release 7.0.

[28] H. C. Roters, *Electromagnetic Devices*. John Wiley and Sons, 1941.

[29] P. Wolters, W. Salber, J. Geiger, and M. Duesmann, “Controlled auto ignition combustion process with an electromechanical valve train,” *SAE paper 2003-01-0032*, 2003.

[30] M. Schechter and M. Levin, “Camless engine,” *SAE paper 960581*, 1996.

[31] J. Xiang, “Modeling and control of a linear electro-mechanical actuator (LEMA) for operating engine valves,” *IEEE Ind. Applicat. Conf.*, vol. 3, pp. 1943–1949, 2002.

[32] G. Amato and M. Meuller-Heiss, “Power stage partitioning for E-VALVE applications,” *SAE paper 2001-01-0239*, 2001.

[33] C.R. Koch and A.F. Lynch and R.R. Chladny, “Modeling and control of solenoid valves for internal combustion engines,” *2nd IFAC Conf. on Mechatronic Systems*, pp. 317–322, 2002.

[34] R. Chladny, “Modeling and simulation of automotive gas exchange valve solenoid actuators,” *M.Sc. thesis, Dept. Mechanical Engineering, University of Alberta*, 2003.

[35] C.R. Koch and A.F. Lynch and S. Chung, “Flatness-based automotive solenoid valve control,” *6th IFAC Symp. Nonlin. Contr. Systems (NOLCOS)*, pp. 1091–1096, 2004.